Effects of thickness ratios and sputtering mode on the structural, electrical and optical properties of bilayer molybdenum thin films

Haili Zhao, Jingpei Xie, Tingting Liang, Aixia Mao, Aiqin Wang, Yanfang Chen, Douqin Ma, Vladislav Paley, and Alex A. Volinsky

Citation: AIP Advances **8**, 095028 (2018); doi: 10.1063/1.5043437
View online: https://doi.org/10.1063/1.5043437
View Table of Contents: http://aip.scitation.org/toc/adv/8/9
Published by the American Institute of Physics

Effects of thickness ratios and sputtering mode on the structural, electrical and optical properties of bilayer molybdenum thin films

Haili Zhao,[1,2] Jingpei Xie,[3,4,a] Tingting Liang,[3] Aixia Mao,[1,2] Aiqin Wang,[3] Yanfang Chen,[3,4] Douqin Ma,[4] Vladislav Paley,[5] and Alex A. Volinsky[5]

[1]*School of Physical Engineering, Zhengzhou University, Zhengzhou 450052, China*
[2]*School of Physical and Engineering, Henan University of Science and Technology, Luoyang 471023, China*
[3]*School of Materials Science and Engineering, Henan University of Science and Technology, Luoyang 471023, China*
[4]*Collaborative Innovation Center of Nonferrous Metals, Henan University of Science and Technology, Luoyang 471003, China*
[5]*Department of Mechanical Engineering, University of South Florida, Tampa, Florida 33620, USA*

(Received 9 June 2018; accepted 12 September 2018; published online 28 September 2018)

In this paper, the bilayer Mo films with a constant thickness were deposited by direct current and direct current (DC/DC), radio frequency and direct current mixed (RF/DC) magnetron sputtering, respectively. Changing thickness ratios of bottom layer to total thickness of bilayer film in the range from 10% to 50%, ten types of bilayer Mo thin films were deposited. The purpose is to improve the photo-conversion efficiency of Cu(In, Ga)Se_2(CIGS) solar cells by changing the sputtering modes and thickness ratio. The microstructures, electrical and optical properties of the bilayer Mo thin films were characterized by scanning electron microscopy (SEM), X-ray diffraction (XRD), atomic force microscope (AFM), Hall Effect measurement system, ultraviolet-visible spectrophotometer (UV-vis) and four-point probe resistance system. It was found that with the increase of thickness ratios in two sputtering modes, both the crystallinity and grain size decreased, while the reflectance increased. Especially, when the thickness ratio was 40%, the resistivity of Mo film prepared in RF/DC mode was as low as 3.365×10^{-5} Ω·cm and the highest reflectance was above 60%. Using this optimized Mo thin film as electrode, the highest photo-conversion efficiency for the CIGS thin film solar cells was as high as 11.5%. https://doi.org/10.1063/1.5043437

I. INTRODUCTION

Molybdenum (Mo) thin films have many excellent properties, such as outstanding electrical conductivity, tuned adhesion on glass by changing sputtering process parameters, and the formation of ohmic contact with CIGSe via unintentionally induced adventitious p-$MoSe_2$ interfacial layer, which have rendered Mo advantages over other investigated metals.[1,2] In addition, Mo thin film affects the out-diffusion of sodium (Na) from soda lime glass (SLG) substrates and iron (Fe) atoms from stainless steel substrates to the CIGS absorber.[3–10] It makes Mo an impeccable choice of back contact, not only for the established CIGS quaternary material,[11,12] but also for the industry standard for novel selenium-free absorber layers, such as Cu_2ZnSnS_4 (CZTS),[13,14] $CuSnS_3$ (CTS) and SnS.[15–19] Processing parameters in-turn affect the residual stress, electrical resistivity, optical reflectance and

[a]Corresponding author: Jingpei Xie; Email: jingpeixie@163.com.

adhesion with SLG.[20] Therefore, an optimization process is necessary to improve the performance of solar cell.

In order to obtain thin films with good conductivity and adhesion, Scofield et al[21] studied the bilayer Mo thin films, which consisted of a bottom layer sputtered at higher sputtering pressure for better adhesion to the substrate and a top layer sputtered at lower pressure for better conductivity. Since then, many studies have focused on the effects of processing parameters on the bilayer molybdenum films, such as the working pressure, sputtering power, substrate temperature, annealing temperature and the discharge power source types.[22,23] However, many researches mentioned above have paid great attentions to the balance between good adhesion and conductivity, but few to the balance between conductivity and reflectance. Actually, the reflectance of Mo back contact layer is also very important to the CIGS, CZTS and other solar cells, because the optimization of back reflection of solar cells can provide non-absorbed light a second chance to be harvested by the active cell layer. Thus, higher reflectance can improve their efficiency.[24] In addition, among these reports, the thickness of bottom layer is also random and the total thickness is uncertain. It is known that the performance of the films will change as the thickness of the bottom layer is altered in the bilayer or multi-layer films.[25] Therefore, changing the thickness ratio of bottom layer to total thickness will have great influences on the performance of bilayer films, such as electrical properties and optical properties.[26] However, to the best of our knowledge, the influence of the thickness ratio of the bottom layer to total thickness on the conductivity and reflectance of Mo thin film has never been investigated systematically.

Herein, the bilayer Mo thin films with fixed total thickness of 600 nm were sputtered on the SLG substrates by using the DC/DC and RF/DC mode, and the electrical properties and reflectance of the films were studied in detail. Specifically, the bottom layers with different thickness were sputtered at higher sputtering pressure in DC and RF modes for better adhesion and reflectance, while the top layers were sputtered at lower pressure in DC mode for better conductivity. The effects of sputtering mode and thickness ratio on the properties of bilayer Mo thin films were systematically investigated. The results show that all bilayer films display good adhesion and conductivity. In especial, the bilayer Mo films, obtained in the RF/DC mode with the thickness ratio of 40%, exhibit higher reflectance and lower resistivity. Using the optimized Mo thin films as electrodes, the highest efficiency of 11.5% was achieved for the CIGS thin film solar cells.

II. MATERIALS AND METHODS

A. Film fabrication

Mo bilayer films were sputtered onto 20mm×20 mm× 1 mm soda lime glass substrates (SLG) using DC/DC and RF/DC magnetron sputtering, with a 99.97% pure Mo target, respectively. The base pressure within the chamber before the deposition process was approximately 2.0×10^{-4} Pa. Before the experiments, the SLG substrates were ultrasonically pre-cleaned using acetone, ethanol and deionized water in sequence, and then dried by blowing with pure N_2 gas (99.99%). Prior to each deposition, the targets were pre-sputtered for 15 min to remove any contamination from the surface of the target. The distance between target and substrate was maintained at 80 mm and all films were grown at room temperature using a water-cooled target. To ensure good surface morphology, all samples were deposited on a rotating substrate. A quartz crystal film thickness gauge was used to control the thickness of Mo thin films during the sputtering process. The parameters and conditions of the sputtering process are listed in Table I.

About 1.5 μm thick CIGS absorbers were deposited on the sputtered Mo electrode/SLG substrates with a 3-stage co-evaporation process.[27] CdS buffer layers grown with chemical bath deposition (CBD) method (~50 nm), sputtered intrinsic zinc oxide (i-ZnO)(~80 nm)/n-type indium tin oxide (ITO) (~250 nm) window layers and evaporated 500 nm thick aluminum (Al) grid electrode were in sequence deposited. The CIGS thin film solar cells with the structure of glass/Mo/CIGS absorber/CdS/i-ZnO/n-ITO/Al were then fabricated. No anti-reflection coating was employed here.

B. Characterization of Mo thin films

The influences of process parameters on the crystallographic properties of the Mo films were observed by X-ray diffraction (XRD, Panalytical, X'Pert Pro) using Cu Kα radiation (0.15406 nm)

TABLE I. The summary of the sputtering parameters.

Sample	Mode (Bottom/Top)	Bottom layer pressure/Pa	Bottom layer thickness/nm	Bottom layer power/W	Top layer pressure/ Pa	Top layer thickness/ nm	Top layer power /W	Thickness ratio of bottom layer
1	DC/DC	1.0	60	100	0.3	540	100	10%
2	DC/DC	1.0	120	100	0.3	480	100	20%
3	DC/DC	1.0	180	100	0.3	420	100	30%
4	DC/DC	1.0	240	100	0.3	360	100	40%
5	DC/DC	1.0	300	100	0.3	300	100	50%
6	RF/DC	1.0	60	120	0.3	540	100	10%
7	RF/DC	1.0	120	120	0.3	480	100	20%
8	RF/DC	1.0	180	120	0.3	420	100	30%
9	RF/DC	1.0	240	120	0.3	360	100	40%
10	RF/DC	1.0	300	120	0.3	300	100	50%

in 2θ scanning mode with 0.02° step size. Scanning electron microscopy (SEM, ZEISS, Merlin) at an operating voltage of 6 kV was performed to characterize the morphology of the sputtered bilayer Mo thin films. An atomic force microscope (AFM, SPA-400) working in tapping mode with a scan peed of 3 Hz and a scan area of 5 μm was used to determine the surface roughness of the films. The reflectance was measured by UV-visible spectrophotometer (Hitachi U-4100) in the wavelength range of 300-1200 nm. The degree of adhesion was qualitatively tested using a Scotch tape test. The electrical parameters, such as carrier concentration and mobility were measured by the Hall Effect measurement system, HMS ECOPIA 3000 with a magnetic field of 0.57 T and probe current of 10 mA for all the samples. The grain sizes (D) of the films was calculated using the Scherrer formula:[28]

$$D = \frac{0.9\lambda}{\beta\cos\theta} \tag{1}$$

Here, λ is the X-ray wavelength (0.15406 nm) and β is the full width at half maximum (FWHM) of the film diffraction peak at 2θ in radians and θ is the Bragg's diffraction angle in degrees. The microstrain, ε and dislocation density, δ developed in the thin films are calculated from Eqs. (2) and (3), respectively[29,30]

$$\varepsilon = \frac{\beta}{4\tan\theta} \tag{2}$$

$$\rho = \frac{n}{D^2} \tag{3}$$

Here, n is a factor, which is almost equal to unity for minimum dislocation density and D is the grain size.

III. RESULTS AND DISCUSSION

A. Crystal structure

Fig. 1 shows the XRD patterns of the Mo films with different thickness ratios of the bottom layer to total thickness, which were deposited in DC/DC and RF/DC modes. All the films exhibit the growth with a preferred orientation along the (110) plane, which is typical for Mo with a body centered cubic (bcc) structure (JCPDS Card No. 3-065-7442). This is ascribed to the fact that the (110) plane of the bcc phase generally has the lowest surface energy and thus it tends to grow preferentially.[31] For the two modes, as the thickness ratio increases, the intensity of the (110) diffraction peak decreases accompanied by the increase of the FWHM. This suggests that the crystallinity of the Mo films is inversely proportional to the thickness ratio. The variation of the FWHM, the grain size, the Hall mobility, the carrier concentration and the roughness of the Mo thin films with different thickness ratios are listed in Table II. It shows that the grain size gradually decreases when the thickness ratio increases from 10% to 50%, which may be due to the number decrease of sputtered atoms with higher energy when the thickness ratio increases. During the sputtering process, the working

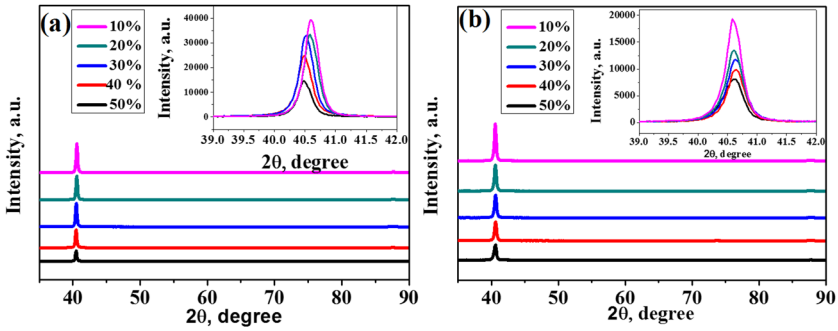

FIG. 1. XRD patterns of Mo films with different thickness ratios deposited in (a) DC/DC and (b) RF /DC modes, respectively, the two insets show their detail information of (110) orientation peaks.

pressure is closely related to the energy of sputtered atoms/ions, and higher pressures enhance the probability of collisions between atoms or ions, leading to the reduction of the atom/ion energy. At very low working pressures, high bombardment energy is delivered to the Mo thin films, resulting in enhanced atomic peening. This can produce denser films and compressive stress. In addition, the higher energy increases atomic mobility and diffusivity, facilitating their nucleation and growth on the substrate.[32] Thus, when the thickness of the Mo films remains unchanged, with the increase of the thickness ratio, the number of sputtered Mo atoms with higher energy is reduced. Then, the surface mobility and diffusivity of the atoms in the whole Mo film are also reduced, correspondingly. Based on the analysis mentioned above, the changes of the properties and microstructures of the Mo thin films deposited with different thickness ratios can be clearly verified.

Moreover, the grain size of Mo thin films deposited in RF/DC mode is smaller than that in DC/DC mode at the same thickness ratio. It can be attributed to lower sputtering rate and lower sputtering kinetic energy of Mo films deposited in RF mode under the same condition. Thus, the grain size and surface roughness are smaller, and the surface is smoother.

Fig. 2a and b show the lattice parameter and strain variations of (110) crystal orientation of Mo thin films with different thickness ratios deposited in DC/DC and RF /DC modes, respectively. Dotted lines in the graphs stand for the equilibrium lattice parameter value, which correspond to 0% strain. For both modes, when the thickness ratio increases, the compressive strain decreases and then turns into tensile strain. Thus, the adherence of Mo thin films to SLG substrate becomes better and better. In addition, it can be clearly seen from Fig. 2a and b that as the thickness ratio increases, the compressive strain decreases, while the tensile strain gradually increases, reaches a maximum value at 40%, and then decreases. It may be that as the thickness ratio increases, the grains size of the Mo films become smaller and the surfaces of the films become flatter and smoother. As a result, the adhesion between

TABLE II. The FWHM for the (110) peak, grain size, Hall mobility, carrier concentration and roughness of Mo thin films with different thickness ratios deposited in DC/DC and RF/DC modes.

Sample	Thickness ratio of bottom layer	Mode (Bottom/Top)	(110) FWHM/°	Grain size/nm	Resistivity/ $\times 10^{-5}$ Ω·cm	Hall Mobility cm^2/Vs	Carrier concentration/ 10^{22} cm^{-3}	Roughness/ nm
1	10%	DC/DC	0.205	44.6	2.522	12.53	16.96	5.36
2	20%	DC/DC	0.244	37.7	2.872	11.82	15.88	5.03
3	30%	DC/DC	0.246	37.0	3.168	11.02	15.26	4.82
4	40%	DC/DC	0.248	36.4	3.246	10.08	15.02	3.85
5	50%	DC/DC	0.251	35.6	3.458	9.52	14.82	2.62
6	10%	RF/DC	0.263	34.9	2.651	11.28	15.40	4.85
7	20%	RF/DC	0.291	31.0	2.983	10.63	14.29	4.50
8	30%	RF/DC	0.294	30.6	3.204	10.23	13.70	4.31
9	40%	RF/DC	0.306	29.3	3.365	9.10	13.63	3.08
10	50%	RF/DC	0.341	26.0	3.802	8.61	13.41	2.36

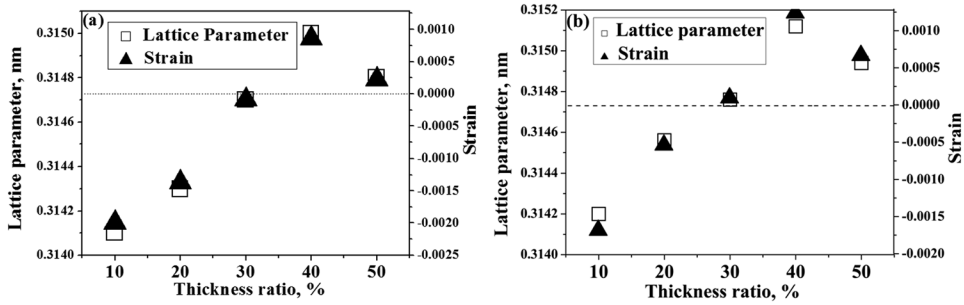

FIG. 2. Lattice parameter and strain variations of (110) crystal orientation of Mo thin films with different thickness ratios deposited in (a) DC/DC and (b) RF /DC modes, respectively.

the film and the substrate becomes stronger, and the compressive strain decreases. In addition, the tensile strain decreases when the thickness ratio is 50%. It originates from the increasing porosity in Mo films due to the more voids.[22] From the results and analysis aforementioned, it can be postulated that both compressive strain and tensile strain are responsible for grain growth in Mo thin films. The decrease in compressive strain increases the physical distance between two or more neighboring grains, which leads to the occurrence of lattice relaxation. Thus, the lattice parameter value is getting closer to the equilibrium lattice parameter value. In addition, the decreasing particle kinetic energy reduces grain boundary migration and in turn facilitates the decrease of grain size. Therefore, it can be concluded that with the increase of the thickness ratio, the adhesion of the films becomes better, the lattice parameter becomes closer to the equilibrium lattice parameter and the grain size becomes smaller.

Additionally, compressive strain for Mo thin films deposited in RF/DC mode is lower than that in DC/DC mode, demonstrating better adhesion of Mo thin films in RF/DC mode. Owing to lower kinetic energy of the films obtained in RF/DC mode, the migration of grain boundary is lower, resulting in smaller grain size, lower compressive strain and higher tensile strain.

B. Surface morphology

Fig. 3 displays the SEM images of Mo thin films with different thickness ratios deposited in DC/DC mode. As shown in Fig. 3a–Fig. 3e, all the films consist of elongated particles with uniform size distribution. With the increase of thickness ratios, the grain size of Mo thin films decreases slightly. In addition, following the reduction of thickness ratios, the surfaces of Mo thin films become rougher, which can be illustrated by AFM, and the root mean square (RMS) roughness is listed in Table II. Specifically, for the Mo thin films deposited in DC/DC mode, the RMS roughness gradually decreases from 5.36 nm to 2.62 nm when the thickness ratios increase from 10% to 50%, which can be attributed to the decrease of grain sizes owing to the fewer sputtered particles with higher energy. It was also reported that lower surface roughness could be obtained for smaller grain cluster due to smaller height difference between a particular grain's peak and base.[33] Cross sections of all Mo films are similar to Fig. 3f, they have columnar structures with the thickness of about 600 nm which are also similar to other reports.[34,35]

Fig. 4 shows the SEM images of Mo thin films with different thickness ratios deposited in RF/DC mode, from which similar results can be obtained as those prepared in DC/DC mode. The films are also composed of elongated particles, and the grain size of Mo thin films decreases slightly with the increase of thickness ratios. When the thickness ratios increased from 10% to 50%, the RMS surface roughness of Mo thin films deposited in RF/DC mode decreases from 4.85 nm to 2.36 nm (see Table II). The films with lower thickness ratios show rougher surfaces. However, for Mo thin film with the thickness ratio of 50%, the number of voids of Mo thin film significantly increases owing to more Mo atoms with lower energy, as shown in Fig. 4e. This will dramatically affect the density and performance of Mo thin film. The cross section of Mo bilayer film prepared in RF/DC mode is shown in Fig. 4f. Again, it exhibits columnar structure.

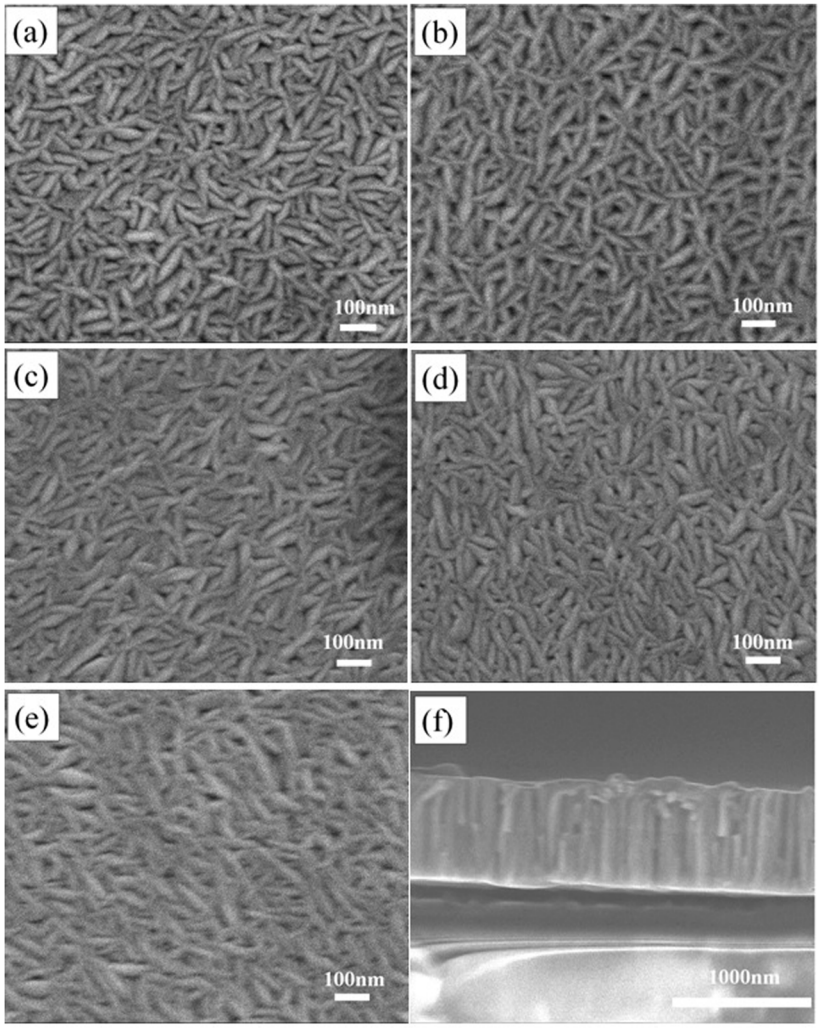

FIG. 3. SEM images of Mo bilayer films deposited in DC/DC mode with different thickness ratios of (a) 10%; (b) 20%; (c) 30%; (d) 40% and (e) 50%, respectively, and (f) the cross section.

It is worth mentioning that the grain size of Mo thin films deposited in RF/DC mode is smaller than DC/DC mode at the same thickness ratio, because the energy of Mo atoms achieved in RF mode is lower than DC mode. Thus, the RMS roughness of the films is also smaller than that in DC/DC mode. Additionally, it can be seen from the cross section that the columnar crystals of Mo thin film deposited in RF/DC mode are smaller than DC/DC mode at the same thickness ratio.

C. Electrical properties

The average microstrain (ε) in Mo thin films, originating from dislocations, was calculated by using Eq. (2), the dislocation density (δ) was calculated from the (110) reflections using the Williamson and Smallman's formula of Eq. (3). The results are represented in Fig. 5. It is clear that both microstrain and dislocation density increase with the increase of thickness ratio, which can directly increase the resistivity of Mo thin films. In addition, it is found from Table II that with the increase of microstrain and dislocation density, the carrier mobility decreases, and the electrical resistivity increases. In fact, the resistivity is caused by the mean squared microstrain. Additionally, there's a linear relationship between microstrain and dislocation density.[36–38] Thus, the resistivity shows a linearly increasing relationship with the increasing dislocation density.[39]

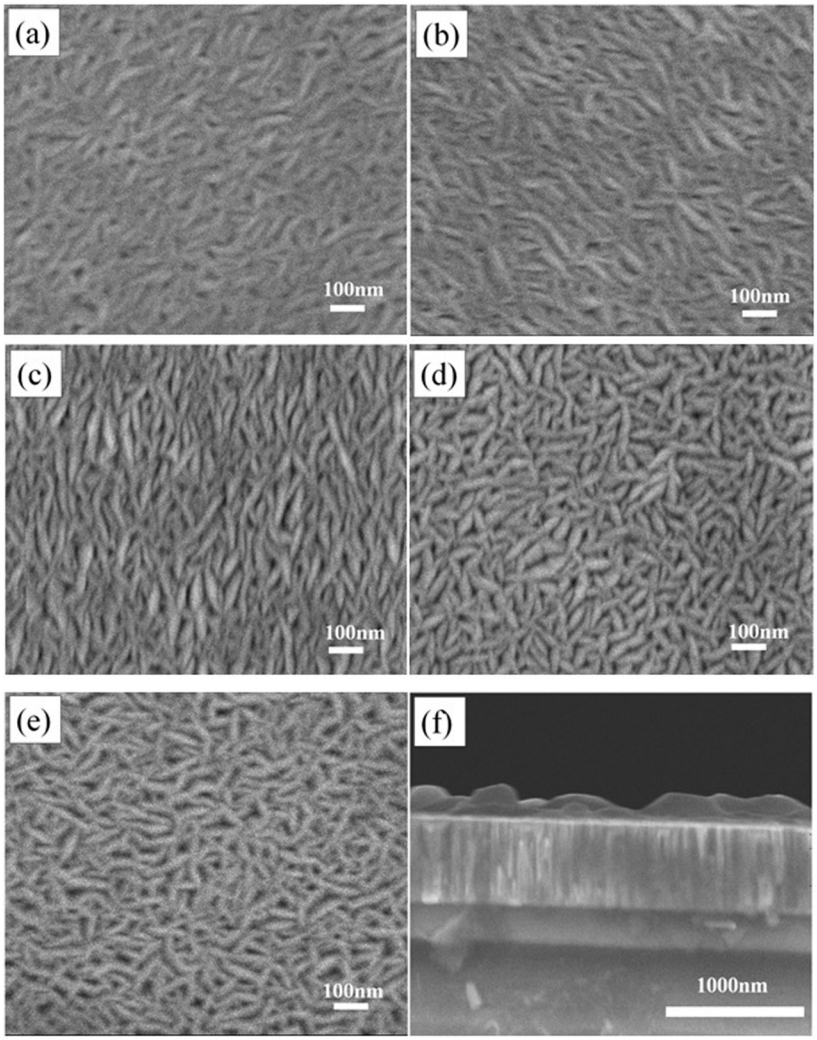

FIG. 4. SEM images of Mo bilayer thin films deposited in RF/DC mode with different thickness ratios of (a) 10%; (b) 20%; (c) 30%; (d) 40% and (e) 50%, respectively, and (f) the cross section.

The electrical properties of Mo thin films are also summarized in Fig. 6. It can be seen that all the resistivity values are larger than that of bulk Mo (ρ_0=5.46×10^{-6} Ω·cm).[40] When the thickness ratios increase from 10% to 50%, the resistivity of Mo thin films deposited in DC/DC mode

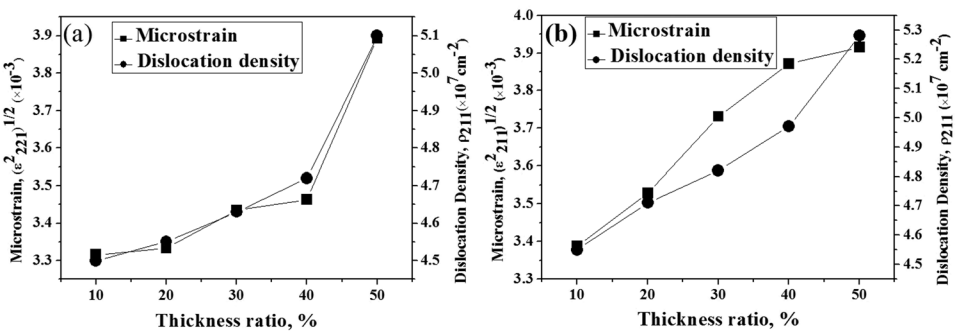

FIG. 5. Microstrain and dislocation density variations of Mo thin films with different thickness ratios deposited in (a) DC/DC and (b) RF/DC modes, respectively.

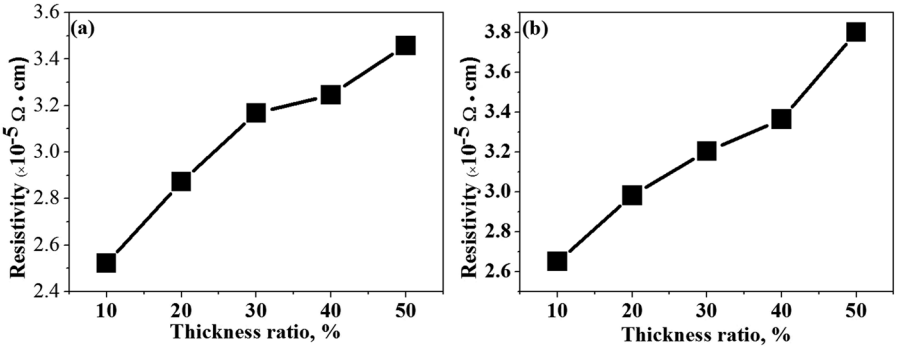

FIG. 6. Resistivity variations of Mo thin films with different thickness ratios deposited in (a) DC/DC and (b) RF/DC modes, respectively.

increases from about 2.5×10^{-5} Ω·cm to 3.5×10^{-5} Ω·cm, while for RF/DC mode, it increases from about 2.7×10^{-5} Ω·cm to 3.8×10^{-5} Ω·cm.

Electron conduction mechanism is dependent on the electron scattering process induced by structural imperfections, such as grain boundaries, dislocation, impurities, microstrain and point defects. In general, a decrease in the grain size in thin films means an increased number of grain boundaries (GBs), where charge carriers have to cross during the electrical transport.[3] At the same time, the grain boundaries in the materials are often considered as the source of dislocations. Therefore, when the thickness ratios increase from 10% to 50%, the grain size decreases, the number of grain boundaries and dislocation density increase, and carrier mobility and carrier concentration decrease. Apart from the decrease in grain size, the randomly distributed dislocation core, which causes resonance scattering of the Fermi electrons, also contributes to the resistivity variation in film through carrier mobility limitation.[41] According to electron scattering theory, the change of resistivity mainly results from the scattering of electrons in atoms around the vacancies or voids at grain boundaries. In this study, as the thickness ratio increases, the grain sizes become smaller and then the more grain boundaries appear. Thus, the more vacancies or voids are formed. Therefore, the electron scattering becomes stronger. In addition, Mo thin films deposited in RF/DC mode have smaller grain sizes, more grain boundaries and stronger electron scattering. Thus, their resistivities are higher than those in DC/DC mode.

D. Optical properties

The reflectance of Mo thin film is also crucial to solar cells efficiency. Maximizing the light reflectance of Mo thin films allows more photons to be absorbed, which is particularly true for submicron CIGS.[42] Fig. 7 shows the reflectance of Mo thin films with different thickness ratios deposited in DC/DC and RF/DC modes, respectively. When the thickness ratios are lower than 40%, Mo thin films with higher thickness ratio of the bottom layers exhibit higher reflectance. The reflectance increases with the increase of the thickness ratio, at 40%, it reaches up to the maximum. Then, with further increase of the thickness ratio, the reflectance decreases instead. These changes are attributed to the decreasing light scattering due to the decreasing surface roughness of Mo thin films. As mentioned above, the surface roughness decreases when the thickness ratios increase. The decrease of roughness can reduce the amount of reflected light perpendicular to the surface. When the thickness ratios increase from 10% to 40%, the reflectance follows this rule exactly. However, the reflectance has an abrupt decrease at 50%, implying that the microstructures of Mo thin film could have an obvious change and result in higher light scattering. The significant change of the microstructure is related to porosity formation along grain boundaries when the thickness ratio of bottom layer is 50% and more voids bring about higher light scattering as shown in Fig. 3e and 4e. Such an evolution of porous structure at the grain boundaries has already been observed from the TEM study of Mo films by Drusedau et al, Mo films deposited at high pressure of 4.7 Pa showed a substantial fraction of inter-columnar voids as large as 10 nm, while those deposited at low pressure

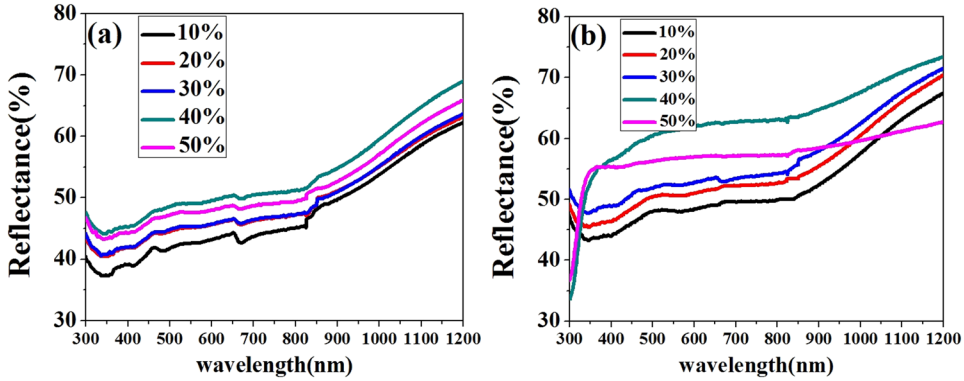

FIG. 7. Reflectance of Mo thin films with different thickness ratios deposited in (a) DC/DC and (b) RF/DC modes, respectively.

of 0.45 Pa exhibited densely packed columns.[43] When the thickness of the whole thin film is keeping constant, increasing thickness ratio of the bottom layer results in the increasing thickness of Mo film deposited at higher pressure, so the porosity becomes higher. These results mean that the optical reflectance is very sensitive to the void formation, but less to the variation in grain size, which is characteristic of the microstructural variation when the thickness ratio is 50%. On the contrary, when the thickness ratio range from 10% to 40%, the optical reflectance is very sensitive to the grain size, but less to the variation in the void formation. It is consistent with the results reported by Yoon et al.[3]

Moreover, Mo thin films deposited in RF/DC mode with same thickness ratio exhibit better reflectance than DC/DC mode. As the grain size of Mo thin film deposited in RF/DC mode is smaller than that in DC/DC mode, the surface roughness and porosity number are reduced. Furthermore, compared with the DC/DC mode, the density and reflectance of the films deposited in RF/DC mode are higher. It originates from that the sputtering rate is lower and the film is more uniform. Thus, the reflectance is higher than the films deposited in DC/DC mode.

As discussed above, for DC/DC mode, when the thickness ratio is 10%, Mo thin films gain the highest conductivity but the lowest reflectance. When the thickness ratio is 40%, the reflectance is the highest, but the conductivity is poor. Additionally, when the thickness ratio of the Mo film deposited in RF/DC is 40%, the resistivity is 3.365×10^{-5} Ω·cm, which is very close to the resistivity of Mo films prepared in DC/DC mode (3.246×10^{-5} Ω·cm), but the reflectance is much higher than that in DC/DC mode.

The CIGS thin film solar cells with the glass/Mo/CIGS absorber/CdS/i-ZnO/n-ITO/Al grid structures are fabricated on the as-prepared Mo electrodes in different sputtering modes with different thickness ratios. Fig. 8 shows the current-voltage (I-V) parameters as a function of thickness ratio and sputtering mode of Mo electrodes. It is found that the open circuit voltage (Voc) is kept relatively constant between 510 mV and 535 mV for all CIGS thin films as shown in Fig. 8a. Fill factor (FF) of CIGS thin films decreases with the increasing thickness ratios of sputtered Mo electrodes, which is related to the increase of resistivity. Short circuit current density (J_{sc}) for the CIGS solar cell with Mo electrodes deposited in RF/DC and DC/DC mode increases with the increase of thickness ratio. The increase of J_{sc} is mainly comes from the light absorption. The photo-conversion efficiency of the CIGS thin film solar cells with Mo electrodes changes in ranging of 9.5-11.5%. Furthermore, for the Mo film with 40% thickness ratio in RF/DC sputtering mode shows excellent comprehensive performance, its resistivity reaches to 3.365×10^{-5} Ω·cm and the reflectance is above 60%. Using this optimized Mo thin films as electrodes, the maximum photo-conversion efficiency of 11.5% is achieved for the copper indium gallium selenium (CIGS) solar cells. The results indicate that under the not obvious difference of the resistivity, the higher reflectance, the higher the photo-conversion efficiency of CIGS solar cells with bilayer Mo films is, while under the not obvious difference of reflectance, the higher resistivity, the higher the photo-conversion efficiency of CIGS solar cells with bilayer Mo films is.

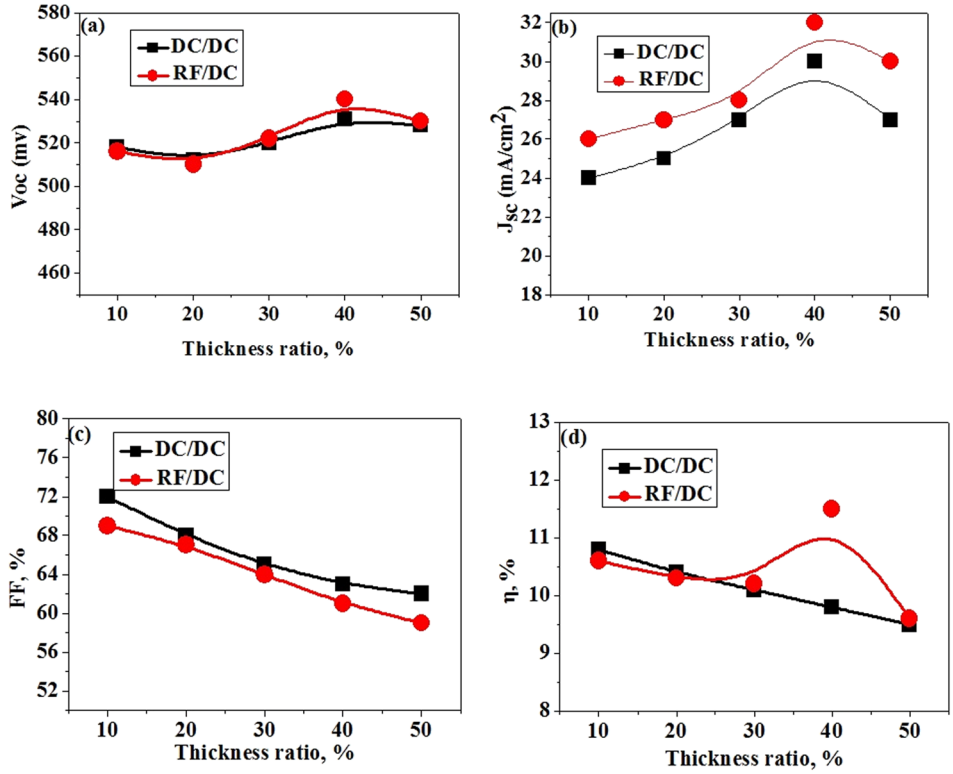

FIG. 8. I-V parameters of CIGS thin film solar cells as a function of thickness ratio of Mo electrodes prepared in RF/DC and DC/DC mode.

IV. CONCLUSION

In summary, the effects of variations in the thickness ratios and sputtering modes of Mo films on the efficiency of a Cu(In, Ga)Se_2 solar cell were investigated. The Mo bilayer films with different thickness ratios were successfully prepared by DC/DC and RF/DC modes. All samples passed the tape tests for adhesion to the SLG substrate, and all of them consist of elongated particles with uniform size distribution. With the increase of thickness ratios, the resistivity of Mo thin film decreases, and the reflectance first increases and then decreases in both sputtering modes. The variations in microstrain and dislocation density show a coherent relationship with the changes of carrier mobility. Optimal film was achieved when the Mo bilayer film thickness ratio was 40% and deposited in RF/DC mode. This bilayer film exhibited extremely low resistivity of 3.365 $\times 10^{-5}\Omega$.cm and highest reflectance of above 60%. A maximum photo-conversion efficiency of 11.5% was obtained for the photovoltaic properties of the completed cells.

ACKNOWLEDGMENTS

The authors acknowledge the support from the Key Project of Education Department of Henan Province (17A430018) and the Key Research Project of Henan Colleges and Universities (18B430008).

[1] N. Kohara, S. Nishiwaki, Y. Hashimoto, T. Negami, and T. Wada, Sol. Energy Mater. Sol. Cells. **67**, 209 (2001).
[2] K. Orgassa, H. W. Schock, and J. H. Werner, Thin Solid Films **431-432**, 387 (2003).
[3] J.-H. Yoon, S. Cho, and W. M. Kim, Sol. Energy Mater. Sol. Cells. **95**, 2959 (2011).
[4] T. Sawaguchi, Prog. Photovolt. Res. Appl. **21**, 58 (2013).
[5] J.-H. Yoon, W. M. Kim, J. K. Park, Y. J. Baik, T. Y. Seong, and J. H. Jeong, Prog. Photovolt. Res. Appl. **22**, 69 (2014).
[6] T. Lepetit, D. Mangin, and E. Gautron, Thin Solid Films **582**, 304 (2015).
[7] P. Blösch, F. Pianezzi, and A. Chirilă, J. Appl. Phys. **113**, 054506 (2013).
[8] Y. C. Lin, D. H. Hong, Y. T. Hsieh, L. C. Wang, and H. R. Hsu, Sol. Energy Mater. Sol. Cells. **155**, 226 (2016).
[9] K. B. Kim, M. Kim, and J. Baek, Electron. Mater. Lett. **10**, 247 (2014).

[10] J. Xu, Z. Cao, Y. Yang, and Z. Xie, J. Mater. Sci.: Mater. Electron. **26**, 726 (2015).
[11] Y. C. Lin, L. C. Wang, K. T. Liu, Y. R. Syu, and H. R. Hsu, J. Alloy Compd. **743**, 249 (2018).
[12] L. R. Zhang, T. Li, and Y. C. Chen, J. Mater. Sci.: Mater. Electron. **29**, 1 (2017).
[13] K. Zhang and H. Guo, J. Mater. Sci.: Mater. Electron. **28**, 17044 (2017).
[14] P. Prabeesh, I. P. Selvam, and S. N. Potty, Appl. Phys. A. **124**, 225 (2018).
[15] B. Shin, O. Gunawan, Y. Zhu, N. A. Bojarczuk, S. J. Chey, and S. Guha, Prog. Photovolt. Res. Appl. **21**, 72 (2013).
[16] J. Koike, K. Chino, and N. Aihara, Jpn. J. Appl. Phys. **51**, 1753 (2012).
[17] P. Sinsermsuksakul, K. Hartman, S. B. Kim, and J. Heo, Appl. Phys. Lett. **102**, 2072 (2013).
[18] K. C. Wang, H. R. Hsu, and H. S. Chen, Sol. Energy Mater. Sol. Cells. **163**, 31 (2017).
[19] A. C. Badgujar, S. R. Dhage, and S. V. Joshi, Thin Solid Films **589**, 79 (2015).
[20] G. Zoppi, N. S. Beattie, J. D. Major, R. W. Miles, and I. Forbes, J. Mater. Sci. **46**, 4913 (2011).
[21] J. H. Scofield, A. Duda, D. Albin, B. L. Ballard, and P. K. Predecki, Thin Solid Films **260**, 26 (1995).
[22] H. M. Wu, S. C. Liang, and Y. L. Lin, Vacuum **86**, 1916 (2012).
[23] J. Feng, W. Zhao, and W. Wei, AIP Adv. **6**, 2 (2016).
[24] O. Poncelet, R. Kotipalli, B. Vermang, A. Macleod, L. A. Francis, and D. Flandre, Solar Energy **146**, 443 (2017).
[25] Y. Kamikawa-Shimizu, M. Watanabe, A. Yamada, and K. Sakurai, Physica Status Solidi. **206**(5), 1063 (2010).
[26] H. Jung, J. Korea Inst. Inform. Commun. Eng. **20**(5), 992 (2016).
[27] A. M. Gabor, J. R. Tuttle, M. H. Bode, A. Franz, A. L. Tennant, M. A. Contreras, R. Noufi, D. G. Jensen, and A. M. Hermann, Solar Energy Mater. Solar Cells **247**, 41 (1996).
[28] A. L. Patterson, Phys. Rev. **56**, 978 (1939).
[29] G. K. Williamson and W. H. Hall, Acta Metallurgica **1**, 22 (1953).
[30] G. K. Williamson and R. E. Smallman, Philos. Mag. **1**, 34 (1956).
[31] Y. C. Feng, D. E. Laughlin, and D. N. Lambeth, J Appl Phys **76**, 7311 (1994).
[32] T. P. Drüsedau, F. Klabunde, P. Veit, and T. H. Hempel, Phys. Status Solidi A. **161**, 167 (1997).
[33] P. Chelvanathan, Z. Zakaria, and Y. Yusoff, Appl.Surf. Sci. **334**, 129 (2015).
[34] P. C. Huang, C. C. Sung, J. H. Chen, C. H. Huang, and C. Y. Hsu, Appl. Surf. Sci. **425**, 24 (2017).
[35] Y. Huang, S. Gao, Y. Tang, J. Ao, W. Yuan, and L. Lu, Thin Solid Films **616**, 820 (2016).
[36] D. Rafaja, H. Köstenbauer, and U. Mühle, Thin Solid Films **528**, 42 (2013).
[37] T. Ungár, I. Dragomir, Á. Révész, and A. Borbély, J. Appl. Crystallogr. **32**, 992 (1999).
[38] M. Wilkens, Phys. Status Solidi. A. **2**, 359 (1970).
[39] B. R. Watts, J. Phys. F: Metal. Phys. **18**, 1197 (1988).
[40] J. P. Moore, R. K. Williams, and R. S. Graves, Rev. Sci. Instrum. **45**, 87 (1974).
[41] R. A. Brown, J Phys. F: Metal Phys. **7**, 1283 (1977).
[42] M. Jubault, L. Ribeaucourt, E. Chassaing, G. Renou, D. Lincot, and F. Donsanti, Sol. Energy Mater. Sol. Cells. **95**, 26 (2011).
[43] T. P. Drüsedau, F. Klabunde, P. Veit, and T. Hempel, Physica Status Solidi **161**, 167 (1997).